Smart Structures and Systems, *Vol. 33, No. 2 (2024) 119-131*
https://doi.org/10.12989/sss.2024.33.2.119

A constrained minimization-based scheme against susceptibility of drift angle identification to parameters estimation error from measurements of one floor

Kangqian Xu [1], Akira Mita [2], Dawei Li [3], Songtao Xue [4] and Xianzhi Li*[1]

[1] *School of Civil Engineering, Qingdao University of Technology, Qingdao, China*
[2] *Department of System Design Engineering, Keio University, Yokohama, Japan*
[3] *School of Civil Engineering, Lanzhou University of Technology, Lanzhou, China*
[4] *Department of Disaster Mitigation for Structures, Tongji University, Shanghai, China*

(*Received May 9, 2023, Revised November 28, 2023, Accepted January 8, 2024*)

Abstract. Drift angle is a significant index for diagnosing post-event structures. A common way to estimate this drift response is by using modal parameters identified under natural excitations. Although the modal parameters of shear structures cannot be identified accurately in the real environment, the identification error has little impact on the estimation when measurements from several floors are used. However, the estimation accuracy falls dramatically when there is only one accelerometer. This paper describes the susceptibility of single sensor identification to modelling error and simulations that preliminarily verified this characteristic. To make a robust evaluation from measurements of one floor of shear structures based on imprecisely identified parameters, a novel scheme is devised to approximately correct the mode shapes with respect to fictitious frequencies generated with a genetic algorithm; in particular, the scheme uses constrained minimization to take both the mathematical aspect and the realistic aspect of the mode shapes into account. The algorithm was validated by using a full-scale shear building. The differences between single-sensor and multiple-sensor estimations were analyzed. It was found that, as the number of accelerometers decreases, the error rises due to insufficient data and becomes very high when there is only one sensor. Moreover, when measurements for only one floor are available, the proposed method yields more precise and appropriate mode shapes, leading to a better estimation on the drift angle of the lower floors compared with a method designed for multiple sensors. As well, it is shown that the reduction in space complexity is offset by increasing the computation complexity.

Keywords: drift angle; multistory shear structure; single sensor-based identification; genetic algorithm; constrained minimization

1. Introduction

Structural performance deteriorates under service loads, and structural damage may occur under accidental loads, such as explosions or earthquakes. Structural health monitoring (SHM) (Mita 2003) has been researched and numerous technologies for diagnosing structures (Fan and Qiao 2011, Das *et al*. 2016) have been developed in the past several decades. Structural identification plays an important role in SHM, because it can provide crucial information for making assessments, including physical parameters (Kuleli and Nagayama 2020), vibration responses (Sun *et al*. 2020), and external forces (Mendrok and Dworakowski 2019). The inter-story drift response, i.e., the difference between the displacements of adjacent floors, reflects structural deformation and reveals the safety status of structures. Hence, the maximum inter-story drift angle is an index that has received a lot of attention.

Displacement responses can be directly detected by using laser sensors (Maksymenko *et al*. 2021, Zhang *et al*. 2020); they can also be extracted from videos or images captured by cameras or smartphones (Xie *et al*. 2021, Shrestha *et al*. 2020, Xu *et al*. 2018, Khaloo and Lattanzi 2017). When the measuring devices are placed outside buildings, the visibility between the instruments and structures will affect the estimation, and sensors and cameras will move together with the ground during an earthquake, which make the identified responses based on the data they acquire unreliable. On the other hand, accelerometers are easy to install and have high precision, and a number of methods have been studied to obtain the displacement from the measured acceleration. The displacement of a floor can be directly computed from the acceleration of corresponding floor by using a high-pass filter (Dan *et al*. 2015), finite impulse filter (Gomez *et al*. 2018), or a frequency-domain integration scheme (Liang *et al*. 2020). In this way, sensors should be placed at all locations of interest. However, in terms of economy, installing a lot of sensors would consume a lot of labor and a complicated SHM system would have a high maintenance cost. That is, a simple sensing system is preferred. Therefore, state-space representations with Kalman filters (Azam *et al*. 2015, Liu *et al*. 2021, Maes *et al*. 2016, Sedehi *et al*. 2019, Valikhani and Younesian 2019) have been researched to estimate the responses of the floors, because the displacement can be related to the acceleration through the equation of motion of the structure. These Kalman-filter

*Corresponding author, Ph.D.,
E-mail: lixianzhi@tongji.edu.cn

http://www.techno-press.org/?journal=sss&subpage=7
ISSN: 1738-1584 (Print), 1738-1991 (Online)

approaches make identifications based on sparse measurements feasible. In other words, it enables a structural evaluation to be implemented and the responses of all stories to be determined by deploying a few sensors on certain floors. Such a simple sensing system can reduce expenses. Moreover, an algorithm developed to work with a few accelerometers can make estimations in extreme situations; for example, sensors may be put out of operation during a strong quake and the amount of recorded data might become inadequate for an estimate to be made using another method.

This study examines two circumstances: (i) subjectively, only a few accelerometers are deployed to reduce costs; (ii) objectively, some sensors fail to record intact responses. If the number of accelerometers is still more than one in either case, there is no obvious difference on the estimation, and the abovementioned approaches (Azam *et al*. 2015, Liu *et al*. 2021, Maes *et al*. 2016, Sedehi *et al*. 2019, Valikhani and Younesian 2019) can be employed. However, if merely one sensor is available, the situation will change. To greatly simplify SHM systems, the authors have tried to use only one accelerometer to estimate the relative displacement and maximum inter-story drift of multi-degree-of-freedom (MDOF) structures (Xu and Mita 2021a, b). In those studies, it was supposed that the modal parameters shift and become unknown when the structure is excited and damaged by a strong earthquake. Here, it is difficult to re-identify the changed modal parameters when measurements are available for only one floor. Single-sensor approaches have been proposed as a way to deal with the unknown parameters. In these approaches, the modal parameters of healthy structures are assumed to have been identified accurately under environmental excitations, which are set as the upper bound of the search range for the variables of genetic algorithm (GA). Then, the shifted unknown frequencies are optimized in the search interval. In addition, another single sensor-based method, that is, an absolute displacement formulation, was developed to reduce the complexity of the state-space model (Xu and Mita 2021c). It was found that the solution of the filters is significantly influenced when the number of sensors goes from many to one, and consequently, prominent differences between the single-sensor and multiple-sensor identifications will arise.

Then, the attention of this study is turned to a practical engineering problem, i.e., estimating the responses of real structures. Since the structural stiffness and damping matrix are difficult to obtain, these unknown structural parameters are often put into a state vector by using physical coordinates and extended Kalman filters (EKF) (Pan *et al*. 2016, Sen and Bhattacharya 2017, Yang *et al*. 2020) or unscented Kalman filters (UKF) (Lei *et al*. 2019, Al-Hussein and Haldar 2016, Wu and Smyth 2007) are used to solve the nonlinear equations. The unknown structural parameters together with the unknown vibration responses usually entail the use of a lot of data to ensure convergence of these physical parameters to the true values and hence obtain a good evaluation of the responses. From the perspective of the modal responses, a great number of approaches have been used to identify modal parameters in the time domain and frequency domain, including stochastic subspace identification (Brewick *et al*. 2018, Van Overschee and De Moor 2012) and frequency domain decomposition (Brincker *et al*. 2001) among others (Kang *et al*. 2021, Mao *et al*. 2019), and consequently, the state-space equation can be expressed using modal coordinates (Azam *et al*. 2015, Maes *et al*. 2016, Li *et al*. 2020). Linear Kalman filters are good for this task. In reality, complex conditions (e.g., measurement noise and environmental effects) induce errors in the identified modal parameters (Astroza *et al*. 2016, Farrar *et al*. 1994). An imprecise model will affect the estimation, but more confidence can be put in the measurements if the amount of data is sufficient. In other words, in the case of the algorithms that take data from multiple sensors, the negative effect resulting from errors in the extracted parameters can be diminished by using many observations of the responses. However, because of the difference between the multiple-sensor and single-sensor scenarios, the performance of these methods will dramatically deteriorate in a circumstance that only the response of one floor is recorded or valid.

Another challenge will be illustrated for the simplest SHM system. If no accelerometer is placed on the base, input signals cannot be acquired when the structures are subject to ground motion. In this situation, the absolute accelerations are monitored and the responses relative to the base are unavailable. Two strategies can be taken. The first is to formulate a dynamic equilibrium equation using the absolute responses (Li *et al*. 2020, Lei *et al*. 2013, Zhao *et al*. 2005). The form of the state-space equation developed from the absolute coordinate system is similar to one expressed in terms of relative responses, but additional steps are required to obtain the relative displacement. In the other strategy, the general equation of motion is utilized to constitute a state-space model (i.e., by using the relative responses), and hence, there is no direct feedthrough term in the measurement equation (Taher *et al*. 2020). The input-augmented class of filters (Nayek *et al*. 2019, Lourens *et al*. 2012) and certain minimum variance unbiased estimators (Valikhani and Younesian 2019) are capable of solving for this kind of problem, but their solutions are vulnerable to errors and noise due to the absence of the direct feedthrough term. Furthermore, single-sensor data will negatively amplify the instability. In summary, when only one accelerometer is available for SHM, the errors in the identified parameters will have a significant effect on the estimation, and the lack of the direct feedthrough term in the measurement equation make the situation worse. Thus, it becomes necessary to develop a single sensor-based approach to estimate the relative displacement and maximum inter-story drift angle based on the identified model by using measurements of one floor.

In this paper, the characteristics of the identification made with only one accelerometer are compared with those of an estimation using many sensors. In particular, only the errors in the measured natural frequencies and mode shapes are considered for the low damped structures. Though changes to the damping ratio should be dealt with carefully when the frequency content of the signal is the same or similar to the structures, more general conditions are considered in the study, that is, changes to the damping ratio

have little impact on the results (Li *et al*. 2020). To obtain a reliable estimation based on an inaccurate identified model from one floor's recorded response, the GA is used to optimize the natural frequencies, as is done in (Xu and Mita 2021a, b). The unknown mode shapes are updated with respect to the frequencies generated by the GA in accordance with the orthogonality relations in reference (Xu and Mita 2021b). Although this method is good at the damage-induced changes to the modal parameters, it is inappropriate for robust estimation (i.e., the structural masses and identified modal parameters are imprecise) of the drift angle of real structures, for two reasons. First, the orthogonality conditions do not hold strictly for structures on site, so the equations may be insoluble. Second, attempting a rigorous solution of the set of equations makes mathematical sense. In fact, the identified natural frequencies and mode shapes may only slightly differ from the real values. However, a small error in the frequencies may lead to a large difference in the computed shapes by solving the equations set. As a result, the calculated mode shapes may be seriously inaccurate. Therefore, two aspects should be taken into account: (i) accuracy (i.e., mathematical aspect): the mathematical relationships between the frequencies produced by the GA and the mode shapes generated with respect to the frequencies should be satisfied as far as possible; (ii) appropriateness (i.e., realistic aspect): the computed mode shapes should not deviate too much from the identified vibrating shapes. A scheme is devised to strike a balance between accuracy and appropriateness and deal with the inexact mode shapes by solving a constrained minimization problem. The proposed algorithm stems from a practical application, so its effectiveness depends on a test on real structures. For this purpose, a full-scale four-story steel structure built at the E-Defense (i.e., a 3-D full-scale earthquake testing facility constructed by Japan's National Research Institute for Earth Science and Disaster Resilience) (2007) was used to validate the method.

The rest of the paper is organized as follows. Section 2 describes the susceptibility of single-sensor identification to the errors in the identified parameters. Section 3 describes the scheme to correct the imprecise mode shapes. Section 4 describes numerical simulations that demonstrate the differences between the multiple-sensor and single-sensor identifications and show the appropriateness of the solution for the mode shapes. Section 5 proves the characteristics of single-sensor estimation and describes the validation of the proposed method using responses measured from a real structure. Section 6 concludes the research.

2. Susceptibility of single sensor identification to parameters error

The absolute acceleration of the *i*th floor of *n*-DOF structures can be determined by superposing the modal velocity and modal displacement. In the case of low damped structures, the terms including the damping ratio can be neglected, and the expression becomes (Xu and Mita 2021a, b)

$$\ddot{u}_i(t) = \sum_{j=1}^{n} \omega_j^2 \phi_{ij} \eta_j(t) = \sum_{j=1}^{n} \omega_j^2 \phi_{ij} \Gamma_j v_j(t) \tag{1}$$

where $\ddot{u}_i(t)$ is the absolute acceleration, ω_j denotes the natural frequency, ϕ_{ij} represents the element of the mass-normalized mode shapes, Γ_j means the participation factor, and $\eta_j(t)$ means the modal coordinates

$$\eta_j(t) = \Gamma_j v_j(t) \tag{2}$$

Here, $v_j(t)$ can be treated as the response of a single-degree-of-freedom (SDOF) structure whose mass, damping coefficient, and stiffness are 1, $2\xi_j\omega_j$, and ω_j^2, respectively (ξ_j is the damping ratio of the MDOF structure). It can be calculated with the Duhamel integral (Clough and Penzien 1993)

$$v_j(t) = \frac{1}{\omega_{Dj}} \int_0^t \ddot{u}_g(\tau) \sin \omega_{Dj}(t - \tau) \exp\left[-\xi_j \omega_j (t-\tau)\right] d\tau \tag{3}$$

where ω_{Dj} is the damped natural frequency, and $\ddot{u}_g(t)$ is the input signal of the SDOF structure (it is also the excitation of the *n*-DOF structure).

At time t_k, the modal response $v_j(t_k)$ can be represented by the input $\ddot{u}_g(t_k)$ by using numerical integration when the modal parameters, the input $\ddot{u}_g(t_{k-1})$, and the responses $v_j(t_{k-1})$ are all known

$$v_j(t_k) \xleftarrow{\text{Numerical integration}\omega_j, \xi_j, v_j(t_{k-1}), \ddot{u}_g(t_{k-1})} \ddot{u}_g(t_k) \tag{4}$$

Accordingly, the *i*th floor's absolute acceleration can be determined from the input

$$\ddot{u}_i(t) = a_{i1} v_1\left(\ddot{u}_g(t)\right) + a_{i2} v_2\left(\ddot{u}_g(t)\right) + \cdots + a_{im} v_m(\ddot{u}_g(t)) + \ldots + a_{in} v_n(\ddot{u}_g(t)) \tag{5}$$

where

$$a_{im} = \omega_m^2 \phi_{im} \Gamma_m$$

In theory, one unknown can be computed in the equation. On the other hand, the modal parameters cannot be accurately identified under complex conditions, and further, measurement noise will affect the solution. If only the first *m* modes are included in the model in an effort to reduce the dimensions of the model, truncation error appears as well. Putting these factors into Eq. (5) yields

$$\ddot{u}_i(t) = a_{i1} v_1\left(\ddot{u}_g(t)\right) + a_{i2} v_2\left(\ddot{u}_g(t)\right) + \cdots + a_{im} v_m(\ddot{u}_g(t)) + \vartheta(t) + \chi(t) + o(t) \tag{6}$$

where $\vartheta(t)$ represents the truncation error, $\chi(t)$ is the modelling error, and $o(t)$ denotes the measurement noise.

When many accelerometers are employed, the expression becomes

$$\begin{Bmatrix} \ddot{u}_i(t) \\ \ddot{u}_p(t) \\ \vdots \\ \ddot{u}_q(t) \end{Bmatrix} = \begin{bmatrix} a_{i1} & a_{i2} & \cdots & a_{im} \\ a_{p1} & a_{p2} & \cdots & a_{pm} \\ \vdots & \vdots & \ddots & \vdots \\ a_{q1} & a_{q2} & \cdots & a_{qm} \end{bmatrix} \begin{Bmatrix} v_1\left(\ddot{u}_g(t)\right) \\ v_2\left(\ddot{u}_g(t)\right) \\ \vdots \\ v_m\left(\ddot{u}_g(t)\right) \end{Bmatrix} + \begin{Bmatrix} \vartheta_i(t) \\ \vartheta_p(t) \\ \vdots \\ \vartheta_q(t) \end{Bmatrix} + \begin{Bmatrix} \chi_i(t) \\ \chi_p(t) \\ \vdots \\ \chi_q(t) \end{Bmatrix} + \begin{Bmatrix} o_i(t) \\ o_p(t) \\ \vdots \\ o_q(t) \end{Bmatrix} \quad (7)$$

As can be seen in Eq. (7), multiple sensors provide more data to make the solution stable. For instance, least squares (LS) can be used to minimize the sum of the squares of the residuals, reducing the influence of the error. When using Kalman filters, a large covariance of process noise can be chosen to put more confidence in the acquired observations. The number of equations decreases as the number of accelerometers decreases, and the effectiveness of the identification will slightly deteriorate. However, once there is only one equation, a sharp change occurs in the performance of the filters because there are no additional data to eliminate the error. In other words, a response estimation using the measurements of one floor is quite vulnerable to errors in the identified parameters, measurement disturbance, and omission of higher modes. To overcome this difficulty, one can increase the time complexity to offset the reduction in space complexity; one scheme to do so is to optimize the natural frequencies (Xu and Mita 2021a, b). The key to this optimization lies in a suitable treatment of the mode shapes, which has a significant impact on the results (Xu and Mita 2021b). Section 3 describes a more appropriate method: constrained minimization.

3. Constrained minimization of mode shapes

If the modal parameters of a structure, including its natural frequencies, damping ratio, and mode shapes, can be accurately obtained, the structural state can be determined even when one accelerometer is deployed. However, it is difficult to obtain accurate modal parameters in practice. Increasing the number of measurements is a simple way to solve this problem since the redundant data can reduce the impact of the modeling error and measurement noise. On the other hand, in the subjective case described in the introduction (i.e., one sensor is installed in the sensing system) or in the objective case (i.e., other devices are disabled to recorded valid data), only one floor's measurements can be accessed after an event. Due to the susceptibility of the single-sensor evaluation to parameters error, a new method is proposed to address the particular situation.

The research (Li *et al*. 2020) indicates that varying the damping ratio within a certain range has little effect on the estimation for law damped structures, so treating errors in the natural frequencies and mode shapes is concentrated on. Here, suppose the parameter identification errors of natural frequencies and mode shapes are α^{id} and β^{id}. The relationship between the identified and true values satisfies

$$\begin{cases} \omega_j^{\mathrm{id}} = \omega_j(1 \pm \alpha_j^{\mathrm{id}}) \\ \phi_{ij}^{\mathrm{id}} = \phi_{ij}(1 \pm \beta_{ij}^{\mathrm{id}}) \end{cases} \Rightarrow \begin{cases} \dfrac{\omega_j^{\mathrm{id}}}{1+\alpha_j} \le \omega_j \le \dfrac{\omega_j^{\mathrm{id}}}{1-\alpha_j} \\ \dfrac{\phi_{ij}^{\mathrm{id}}}{1+\beta_{ij}} \le \phi_{ij} \le \dfrac{\phi_{ij}^{\mathrm{id}}}{1-\beta_{ij}} \end{cases} \quad \alpha_j \ge \alpha_j^{\mathrm{id}}, \beta_j \ge \beta_j^{\mathrm{id}} \quad (8)$$

where the superscript id means the identified data, α_j and β_j are custom data ($\alpha_j,\ \beta_j > 0$), which are treated as error bounds.

The study aim is to minimize the difference between the recorded response and the response estimated from the fictitious frequencies $\widetilde{\boldsymbol{\omega}}$ and mode shapes $\widetilde{\boldsymbol{\Phi}}$. The genetic algorithm (GA) can treat the frequencies as individuals and generate H groups of frequencies randomly within the ranges (the first expression in Eq. (8)), and the root mean square (RMS) of the two responses together with the innovation term in the Kalman filter is used as the fitness function (Xu and Mita 2021a, b) (see Fig. 1). For the fictitious mode shapes, n^2 elements need to be addressed. Regarding these unknowns as GA variables (i.e., including n^2 unknowns for modes shapes and n knowns for frequencies) will increase the complexity of the optimization. Here, full advantage should be taken of the relation between the generated frequencies and the mode shape to be solved. In the research (Xu and Mita 2021b), the natural frequencies and mode shapes are assumed to be shifted by severe damage to the structure under a strong earthquake, and the mass and stiffness orthogonality conditions are used to update the corresponding mode shapes $\widetilde{\boldsymbol{\Phi}}^{[h]}$ with respect to the hth group of frequency variables $\widetilde{\boldsymbol{\omega}}^{[h]}$ in the GA by solving a set of nonlinear equations. This approach is mathematically correct but not physically correct for the case of imprecise identified parameters. A small alteration of the frequencies may result in a different mode shapes solution, and even the calculated shapes seriously violate the second expression in Eq. (8). Moreover, the orthogonality relations cannot be satisfied rigorously because of the complexity of real structures. For example, the vibrating shapes will be not completely orthogonal to the stiffness matrix. As a result, the solutions to the nonlinear equations are sometimes invalid.

To ensure the accuracy, the computed mode shapes must satisfy the mathematical relationships with the frequencies generated by the GA as much as possible. From the perspective of the realistic aspect, it requires the calculated shapes to be in the appropriate range. This following is a more reasonable scheme to handle the inaccurate mode shapes arising from the parameter identification error, balancing the accuracy and appropriateness. The orthogonality conditions in modal form for the hth group of frequencies in GA can be described as

$$\begin{aligned} \boldsymbol{M} &= (\widetilde{\boldsymbol{\Phi}}^{[h]}\widetilde{\boldsymbol{\Phi}}^{[h]^T})^{-1} \\ \widetilde{\boldsymbol{K}}^{[h]} &= \boldsymbol{M}\widetilde{\boldsymbol{\Phi}}^{[h]}\widetilde{\boldsymbol{\Lambda}}^{[h]}\widetilde{\boldsymbol{\Phi}}^{[h]}\boldsymbol{M} \end{aligned} \quad (9)$$

where

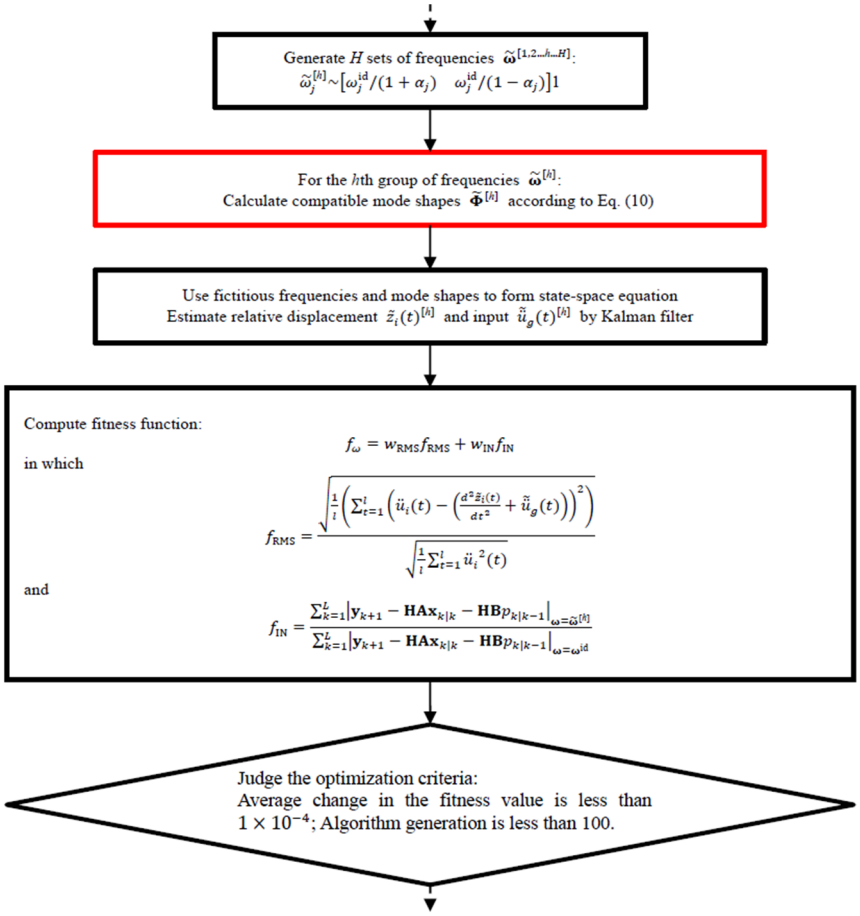

Fig. 1 Genetic algorithm (GA) to optimize frequencies with the help of correcting the mode shapes

Note: $\tilde{\boldsymbol{\omega}}$ is the frequencies generated in GA, H is the number of GA population, $\tilde{\boldsymbol{\Phi}}$, $\tilde{z}_i(t)$, $\tilde{\ddot{u}}_g(t)$ represent the mode shapes, relative displacement, and input estimated by $\tilde{\boldsymbol{\omega}}$, $\ddot{u}_i(t)$ is the measured absolute acceleration, f_ω is the fitness, and the details of structural analysis are shown in Appendix A

$$\tilde{\boldsymbol{\Lambda}}^{[h]} = \mathrm{diag}\left((\tilde{\omega}_1^{[h]})^2 \quad (\tilde{\omega}_2^{[h]})^2 \quad \cdots \quad (\tilde{\omega}_n^{[h]})^2\right)$$

The stiffness matrix of a real structure is unavailable, but its properties for shear structures can be utilized, that is, except for the first row of the matrix, the sum of the remaining rows equals zero theoretically. The elements of the mode shapes are assumed to vary within the deviation ranges of the identified values, which can be employed as constraints. Hence, the problem of solving for unknown mode shapes transforms into a constrained minimization problem, where the imprecise vibrating shapes extracted from the responses of the structures under natural excitations are set to the initial values, as shown in Eq. (10). It is worth noting that Eq. (10) will fail to accurately calculate the mode shapes when the stiffness matrix of other type of structures is not a tridiagonal matrix.

$$\begin{aligned}&\tilde{\boldsymbol{\Phi}}^{[h]} \\ &= \underset{\tilde{\boldsymbol{\Phi}}^{[h]}}{argmin}\left\{\sum_{row=1}^{n}\left|\sum_{column=1}^{n}\left[(\tilde{\boldsymbol{\Phi}}^{[h]}\tilde{\boldsymbol{\Phi}}^{[h]^T})^{-1} - \boldsymbol{M}\right]\right| \right. \\ &\left. + \sum_{row=2}^{n}\left|\sum_{column=1}^{n}\left[\boldsymbol{M}\tilde{\boldsymbol{\Phi}}^{[h]}\tilde{\boldsymbol{\Lambda}}^{[h]}\tilde{\boldsymbol{\Phi}}^{[h]}\boldsymbol{M}\right]\right|\right\}\end{aligned} \quad (10)$$

$$\text{Subject to: } \left\{\text{Inequality constraint: } \phi_{ij}^{\mathrm{id}}/(1+\beta_{ij}) \le \tilde{\phi}_{ij}^{[h]} \le \phi_{ij}^{\mathrm{id}}/(1-\beta_{ij})\right\} \quad (10)$$

The implementation of the GA in the proposed method is illustrated in Fig. 1. When the optimization criteria are met, the GA determines the optimized natural frequencies $\boldsymbol{\omega}^{\mathrm{opt}}$, and Eq. (10) can then be used to calculate the final optimized mode shapes $\boldsymbol{\Phi}^{\mathrm{opt}}$ with respect to the optimized frequencies. The errors in the identified parameters can be reduced by increasing the computational time, and thereby a more exact model is acquired to evaluate the relative displacement from the measurements of one floor. The error bounds, α_j and β_j, of the natural frequencies and mode shapes, should be set carefully. Wide error ranges ensure that the optimized parameters can converge to the true value, and the details are shown in the research (Xu and Mita 2021a). Because the ith floor's response is the object of the optimization, the estimated displacement of that floor has high accuracy. When the accelerometer is deployed on the first floor, the maximum inter-story drift angle can be precisely calculated from the absolute acceleration since the drift response of the first floor is the relative displacement. The precisions of the determined drift angles of the floors

above the first will deteriorate but normally those of the lower floors (i.e., the second, third, etc.) will be less affected because these stories are closer to the sensor and the mode shapes are solved more appropriately by using the constrained minimization. In the case of shear structures, the inter-story drift of the lower floors is usually considered to be the most important for identification purposes owing to their large values, and the proposed approach is suitable for such applications.

4. Numerical simulations

To examine the difference between multiple-sensor and single-sensor identifications, simulations on a six-story shear structure are conducted. As well, the effectiveness of the constrained minimization method in solving for the mode shapes was investigated in numerical simulations. As shown in Fig. 2, the masses of the bottom and top floors are 1100 and 900 tons, and other floor's masses are 1000 tons. The inter-story stiffness linearly decreases from 2.5×10^6 kN/m to 2.0×10^6 kN/m. The story heights are all 3.0 m. The damping ratios in the first two modes are set to 2% and 3% for the low damped structures, and the damping ratios of the other modes are Rayleigh damping. The EI Centro earthquake signal is used to excite the structure.

4.1 Difference in estimated relative displacement between using multiple sensors and using a single sensor

Here, the number of accelerometers and error level are changed to examine the effect of varying the number of the measurements on the estimated relative displacement based on the roughly identified parameters. It is supposed that the error of the parameter identification obeyed a normal distribution, that is $\varepsilon \sim N(\mu, \sigma^2)$ and set the standard deviation of the identification error to $\sigma = 5\%$. The sensor layouts listed in Table 1 are analyzed. The errors are produced randomly and independently and added to each element of the natural frequencies and mode shapes (in particular, the error is introduced to the mode shapes node by node). The state-space representation is formed by these inaccurate modal parameters, and the absolute acceleration responses of corresponding stories are treated as observations. The relative displacements of all floors are determined with a linear Kalman filter. To obtain reliable results, the above procedure (it includes four steps, generating errors, polluting the modal parameters element by element, formulating the state-space equation by the imprecise parameters, estimating the relative displacements by the Kalman filter) are repeatedly carried out for one hundred times. The averages of the estimated displacements are shown in Fig. 3. What stands out in this graph is the difference between the multiple-sensor and single-sensor identifications. The errors are basically consistent when the number of sensors is more than three, and they slightly increase when two accelerometers are used. However, the errors of the estimation steeply increase when only one accelerometer is used, which shows the susceptibility of an identification based on a single sensor to modelling error. In addition, the results of different floors show subtle differences depending on the location of the accelerometers. When one accelerometer is installed on the first floor, the accuracy for the higher stories gradually decreases as the stories are far away from the sensor. The evaluation of the floors whose absolute responses are detected is more accurate than those of the floors on which no sensor is deployed; for example, the deviation of the estimate for the sixth floor is smaller than that of the fifth floor in the case of two, three, and four accelerometers.

Now the error levels in the identified modal parameters are discussed. To exhibit the difference and tendency of response estimation using different numbers of accelerometers clearly, the standard deviations σ of 2%, 5%, 10%, and 15% are considered, and the relative error of the inter-story drift angle of the first floor is illustrated in Fig. 4. Large difference between singe-sensor and multiple-sensor identifications can be observed, that is, the

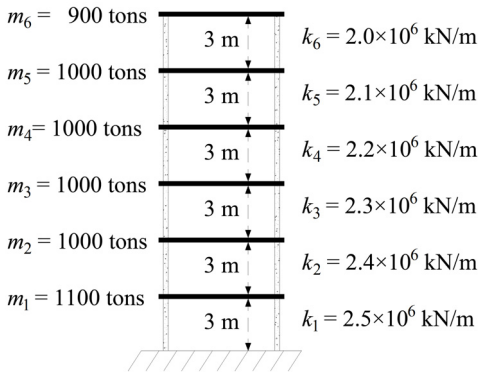

Fig. 2 Six-story shear structure

Table 1 Sensor configurations

Number of sensors	Installation floor
1	1st floor
2	1st and 6th floors
3	1st, 3rd, and 6th floors
4	1st, 3rd, 4th, and 6th floors
5	1st, 2nd, 3rd, 5th, and 6th floors
6	1st, 2nd, 3rd, 4th, 5th, and 6th floors

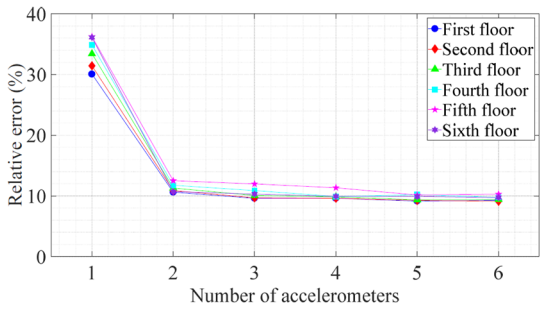

Fig. 3 Relative error of estimated displacement of floor versus number of installed accelerometers (standard deviations is 5%)

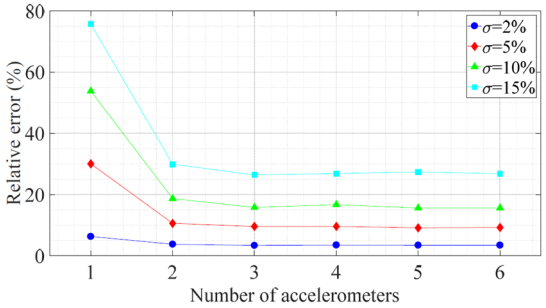

Fig. 4 Relative error of drift angle of first floor versus sensor number and error levels

identifications based on a single sensor clearly have more error than those based on many sensors: the estimation errors substantially change when the number of stories with installed accelerometers goes from even two to one. As the error level increases, the single sensor-based identification is more strongly affected than the multiple sensor ones: the percentage error of the estimated drift angle of the first floor grows at a faster rate than those of the multiple sensor estimations, e.g., from 6.31% to 30.06% for one sensor and from 3.81% to 10.60% for the two accelerometers as the standard deviation σ goes to 5% from 2%. Thus, the single sensor-based solution is quite susceptible to errors in the modal parameters, and hence, a special algorithm should be investigated to deal with the problems in engineering. It is worth noting that the relative errors of estimation are still unacceptable in the case of more than one accelerometer when the standard deviation of parameter identification is more than 2%. Therefore, better parameter identification is necessary to make a good estimation, though the responses of many floors are measured.

4.2 Appropriateness of the solution for the mode shape

The first two columns of Table 2 list the modal parameters that have been polluted at an error level of $\sigma = 5\%$, which are treated as the identified natural frequency and identified mode shape. The error bounds α and β are set to 10%. The proposed method in Section 3 is used to correct the imprecise mode shapes by solving a constrained minimization problem, and the result is the minimization-based mode shape. For comparison, the equation-based mode shapes are obtained on the basis of a set of nonlinear equations (Xu and Mita 2021b). After the GA is run, the approximate mode shapes corresponding to the optimized frequencies are acquired by running the update program of the mode shapes again. The mode shapes are shown in Fig. 5. The modal assurance criterion (MAC) value is used to quantify the results between the actual mode shapes ϕ_j^{act} and other mode shapes ϕ_j^{oth} (including the identified, minimization-based, and equation-based mode shapes). The MAC value is calculated by Eq. (11), and the closer the value is to 1, the better the correlation. The reslts are listed in Table 3. Evidently from Fig. 5 and Table 3, when the mode shapes are updated using the set of equations, the calculated values are not consistent with the theoretical

Table 2 Two groups of identified natural frequencies (first three modes)

σ = 5%		σ = 10%	
Natural frequency (Hz)	Relative error (%)	Natural frequency (Hz)	Relative error (%)
1.96	3.61	1.75	7.07
5.61	4.29	5.58	3.86
7.84	7.84	9.07	6.56

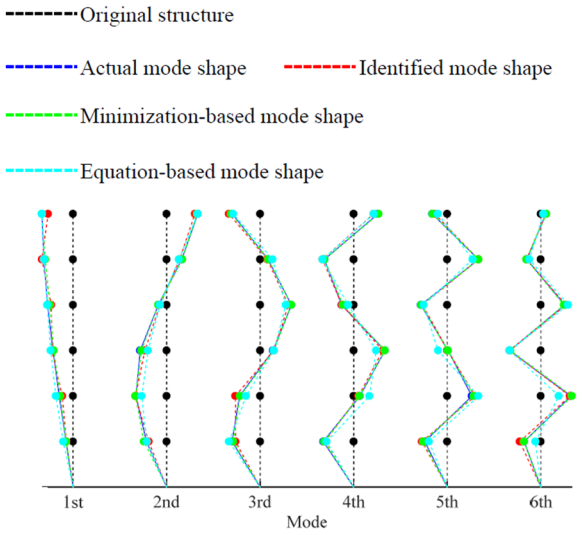

Fig. 5 Comparison of mode-shape solutions

shapes, even though the orthogonality conditions are satisfied exactly. On the other hand, by using the constrained minimization scheme to determine the mode shapes, the mode shapes are not strictly orthogonal to the mass and stiffness matrix, but they are closer to the actual vibrating shapes (i.e., the average of Eq. (12) is not zero, approximate 0.03). In this sense, the constrained minimization approach makes a great improvement to the mode shapes.

$$\text{MAC}\left(\phi_j^{\text{act}}, \phi_j^{\text{oth}}\right) = \frac{\left|\phi_j^{\text{act}^*}\phi_j^{\text{oth}}\right|}{\sqrt{\phi_j^{\text{act}^*}\phi_j^{\text{act}}}\sqrt{\phi_j^{\text{oth}^*}\phi_j^{\text{oth}}}} \tag{11}$$

where the superscript "*" is the complex conjugate transpose.

$$\begin{aligned}\text{Orthogonality}\ \left(\phi_p, \phi_q, M\right) &= \frac{\left|\phi_p^T M \phi_q\right|}{\sqrt{\phi_p^T\phi_p}\|M\|_2\sqrt{\phi_q^T\phi_q}} \\ \text{Orthogonality}\ \left(\phi_p, \phi_q, K\right) &= \frac{\left|\phi_p^T K \phi_q\right|}{\sqrt{\phi_p^T\phi_p}\|K\|_2\sqrt{\phi_q^T\phi_q}}\end{aligned} \tag{12}$$

where $p \neq q$, $\|\ \ \|_2$ is the 2-norm.

Actual mode shape is the analytic solution; Identified mode shape means the polluted parameters by errors; Minimization-based mode shape is the result determined by the proposed method (Eq. (10)); Equation-based mode

Table 3 MAC values between actual mode shapes and other mode shapes

Type / MAC / Order	Identified mode shapes	Minimization-based mode shapes	Equation-based mode shapes
1st	0.991365	0.999462	0.996875
2nd	0.996816	0.998717	0.990945
3rd	0.991854	0.999460	0.983920
4th	0.996340	0.999578	0.966542
5th	0.995708	0.999209	0.960644
6th	0.996696	0.999507	0.951916

shape is calculated based on a set of nonlinear equations (Xu and Mita 2021b).

The first three optimized frequencies are displayed on the left side of Fig. 6(a). The error in the measured parameters reduces with the cooperation of the more appropriate mode shapes. The estimated drift angle of the first floor is determined using the optimized parameters and the measurements of this floor. For comparison, estimations were also made on the basis of the identified model in the case of deploying one accelerometer or six sensors. The results are shown on the right side of Fig. 6(a). The model using the imprecise identified frequencies give a poor estimate of the drift angle when the measurements of only one floor are utilized, while it gives better estimates as the number of accelerometers is increased. On the other hand, when data from only one accelerometer is available, the model with the optimized frequencies and updated mode shapes has a significantly smaller error, although the converged frequencies are worse for the third mode than for the first two modes. Fig. 6(b) depicts the results for another set of extracted frequencies (listed in the two columns on the right of Table 2) to which errors with $\sigma = 10\%$ are added. Here, it can be seen that there is a limited enhancement in making more measurements. On the other hand, the proposed method obtains a better evaluation within this larger deviation range. It should be noted that GA requires a larger population to avoid local convergence at high error levels, and hence, its computational time grows a little. The estimation of drift angle using the proposed method consumes about 20 minutes, whereas the direct estimation using the Kalman filter without the parameters optimization by GA needs less than 1 minute. In summary, the aim to improve the estimation accuracy can be reached by the proposed approach.

IdFre-1 means an estimation using the identified frequencies and data from one sensor; IdFre-6 means an estimation using the identified frequencies and data from six sensors; OpFre-1 means an estimation using the optimized frequencies and data from one sensor.

5. Validation on a real structure

A real structure is used to validate the proposed approach. Section 5.1 describes the shear building used in the test. Section 5.2 shows the vulnerability of an estimation based on one accelerometer. Section 5.3 examines the appropriateness of the mode shapes determined by the constrained minimization method and the estimated precision of the drift angle.

5.1 Test Building

A full-scale four-story steel structure was built and tested at E-Defense, which is part of Japan's National Research Institute for Earth Science and Disaster Resilience (2007). A photo of the building and illustrations of its appearance and structure are shown in Fig. 7. The structure had two spans 2 × 5 m = 10 m in the long-side direction (y-axis) and one span (6 m) in the short-side direction (x-axis). The lumped masses of the first to fourth floors were 47.45, 47.30, 47.65, and 63.15 tons. A total of 75 accelerometers (model number: TA-25E-10-1, maker: TOKYO KEIKEI) were placed at the four corners and the center of the shake table and the floors. Three laser sensors (model number: LK-500, maker: KEYENCE) are installed in each story to record the inter-story drift responses; two sensors measured in the longitudinal direction, the other the transverse direction. In this study, the motion along the longitudinal direction of the building is focused on and used only the measurements from the accelerometers at the center of each floor and base. The average drift response measured by the two displacement meters along the y-axis was used as a reference for comparison with the results estimated from the absolute acceleration. The deployed sensors are plotted in the floor plan in Fig. 8; the utilized accelerometers and displacement meters are colored red and blue, respectively.

At the first stage, the four accelerometers installed at the center point of each floor are considered. In practice, stochastic subspace identification (SSI) (Van Overschee and De Moor 2012) can be used to extract the modal parameters from detected responses to wind loads or small earthquakes. The closer the load is to white noise, the better SSI performs. In the test to identify the dynamic properties, acceleration responses to the earthquake were used instead of responses to white noise, which is a less than ideal

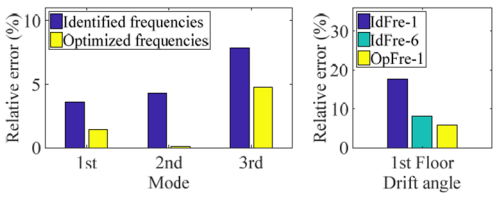

(a) Error level of $\sigma = 5\%$ in identified parameter

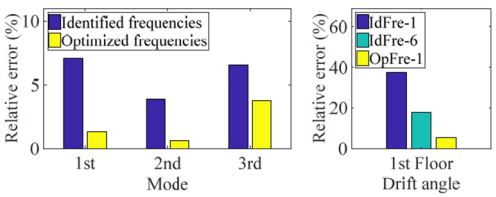

(b) Error level of $\sigma = 10\%$ in identified parameter

Fig. 6 Optimization of imprecise parameters and estimation error of first floor's drift angle

(a) Photo of the building

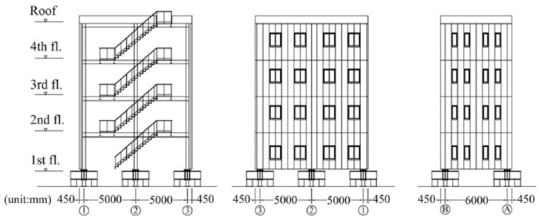

(b) Appearance of the building

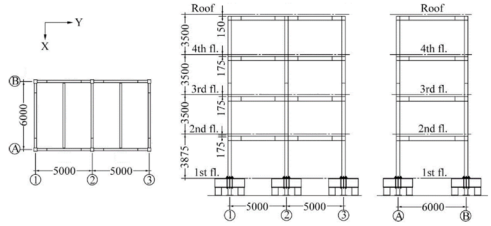

(c) Structure views

Fig. 7 Full-scale four-story steel structure

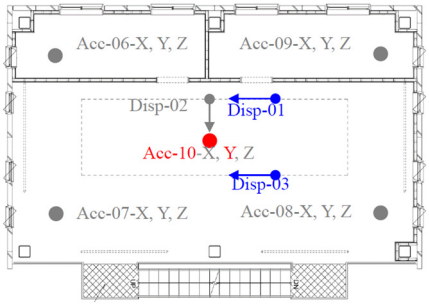

Fig. 8 Locations of accelerometers and displacement meters on the first floor plan

condition. The SSI program was used to identify the parameters for model orders from 2×4 to 2×30. The identified frequencies are plotted with respect to the model order in Fig. 9; the power spectral density (PSD) of the first floor's response is also shown. Spurious and redundant modes appear at higher model orders. Intuitively, four stable modes appear around the peak of the PSD. The rate of change of the modal parameters identified from adjacent

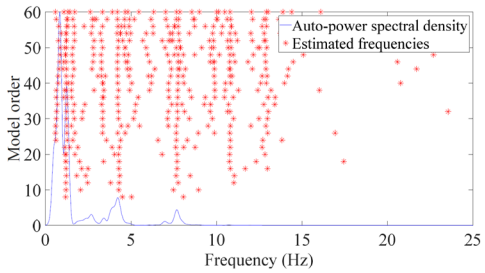

Fig. 9 Parameters identified by SSI

model orders can be utilized as a criterion to get rid of these noise modes, as shown in Eq. (13). (Brewick *et al*. 2018). It can be seen that the frequencies fluctuate with the model order, meaning a non-ideal case. A group of modal parameters are chosen, and the identified natural frequencies of the first four modes are 1.36, 4.33, 7.62, and 10.80 Hz.

$$\begin{aligned} &\frac{|\omega_{r+2}-\omega_r|}{\omega_r} < 0.01 \\ &\frac{|\xi_{r+2}-\xi_r|}{\xi_r} < 0.05 \\ &\frac{|\phi_{r+2}^{*}\phi_r|}{\left(\sqrt{\phi_r^{*}\phi_r}\sqrt{\phi_{r+2}^{*}\phi_{r+2}}\right)} > 0.98 \end{aligned} \tag{13}$$

5.2 Single-sensor and multiple-sensor estimations

Structural assessments can be performed on buildings whose parameters have been identified and which have been equipped with sensing systems. Here, the four accelerometer configurations listed in Table 4 were investigated. The building was subject to a 10% JR Takatori earthquake wave. The input signal is shown in Fig. 10. The structural responses to the input between the two red lines were analyzed. The sampling frequency of the accelerometers was 1000 Hz, and resampling was performed on the recorded responses at 100 Hz. The extracted parameters were incorporated in a state-space model and estimations were made from the recorded absolute accelerations. The time history of the responses and the relative errors of the peak values obtained under different conditions are displayed in Figs. 11 and 12. Regarding the first floor's drift response, the three response identifications cases in which multiple accelerometers were used are similar to each other, and their time histories are in accord with the monitored displacement. However, the single-sensor estimation deviates the time history of displacement response recorded during the quake. The maximum displacements in Fig. 12(b) are similar to those of the simulations, that is, the error is much smaller when at least two accelerometers are used than when only one sensor is employed, and it slowly decreases as the number of accelerometers increases for the multiple-sensor estimation. What is different from the simulations is that the influence of the location of the sensors on the floors' responses estimation is not as obvious. In Fig. 12(a), the peak inter-story drift gradually decreases going from the first floor to the top floor, but the maximum drift angle

appears at the second story due to its smaller height. The drift response of the first floor was directly calculated from the estimated structural state since it equals the relative displacement of the floor. The other floors' inter-story drift can be computed from the evaluated displacement of the adjacent stories, and error will accumulate in the differences. It can be seen in Fig. 12(c) that the drift angles of the second floor and third floor are obtained with high accuracy in the multiple-accelerometer cases. The precision on the top floor can be improved when many accelerometers are deployed, but it is still poor because the inter-story drift of the fourth floor is small relative to other floors.

Table 4 Sensor layouts

Number of sensors	Installation floor
1	1st floor
2	1st and 4th floors
3	1st, 2nd, and 4th floors
4	1st, 2nd, 3rd, and 4th floors

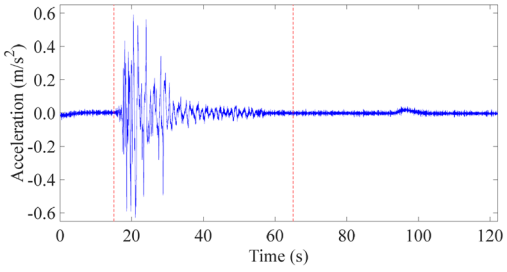

Fig. 10 Input signal

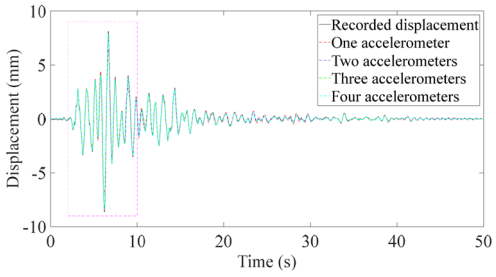

(a) Whole time history

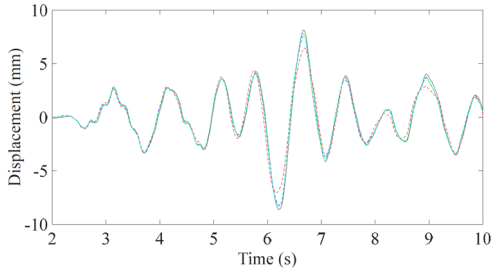

(b) Stretched image of window defined by the dotted lines in (a)

Fig. 11 Inter-story drift response of first floor estimated using different sensors

5.3 Improvement for the one-accelerometer case

In this study, suppose that only one accelerometer was deployed on the first floor to service for SHM. After the absolute response of the first floor was recorded, the proposed method was implemented. The mode shapes calculated by the constrained minimization with respect to the optimized frequencies are plotted in Fig. 13, together with values obtained by solving equations set (i.e., the algorithm in (Xu and Mita 2021b)). Although the method from (Xu and Mita 2021b) is competent to estimate the peak inter-story drift for the severe damaged structures, here, it fails to give reasonable mode shapes in the case of the inaccurate identified parameters. On the other hand, the proposed method can balance the mathematical aspect and the realistic aspect, and hence, it obtains accurate results of mode shapes. Fig. 14 shows the inter-story drift of the first floor. The estimate using the optimized frequencies and corresponding mode shapes better matches the detected response than does the estimate using the identified parameters in the case of using one accelerometer. Although the estimation based on four sensors was the most accurate, as mentioned before, the proposed method can offset the impact induced by the insufficient data by increasing the

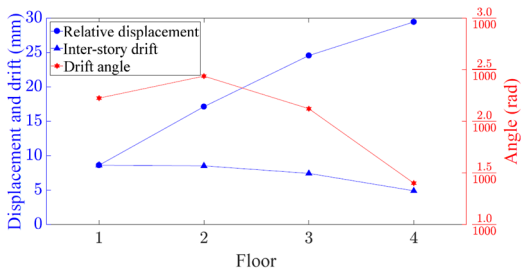

(a) Maximum relative displacement, inter-story drift, and drift angle of each floor

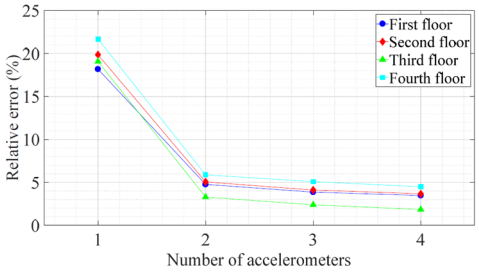

(b) Estimated relative displacement

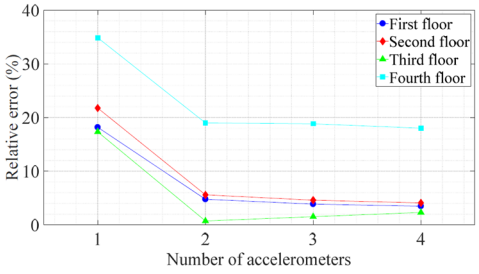

(c) Estimated drift angle

Fig. 12 Percentage error of peak displacement and drift angle

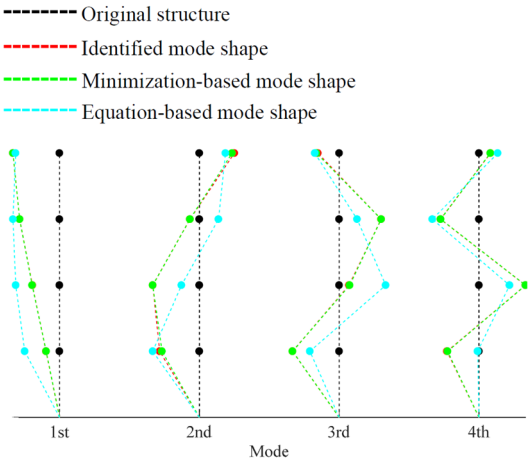

Fig. 13 Mode shapes computed using different methods

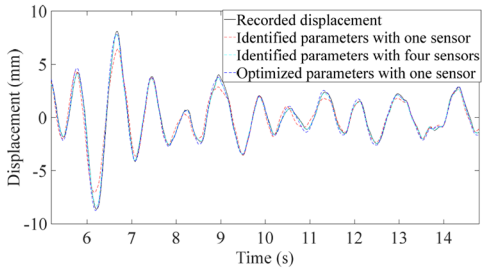

Fig. 14 Time history of inter-story drift of the first floor

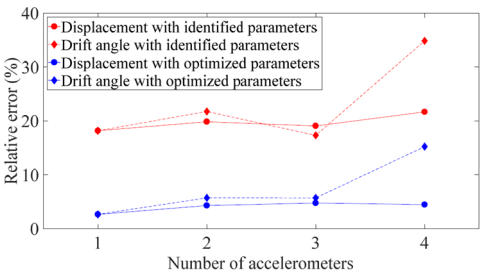

Fig. 15 Relative error of maximum relative displacement and drift angle

computational time. The relative errors of the peak relative displacements and drift angles of all stories are shown in Fig. 15. The proposed method improves precision in all cases. In detail, the drift angle for the first floor is the best because its acceleration response is the optimization objective. The estimates for the second story and third story are also good because of the more appropriate mode shapes. On the other hand, the results for the fourth floor are poor since the top floor has a minor deformation and it is far away from the sensor. The largest inter-story drift and drift angle occur in the first story and second story, so the estimated responses of these floors are most important. These results show that the proposed approach can accurately determine the drift angles of the lower floors from the measurements of the first floor.

6. Conclusions

This paper showed the difference between single-sensor and multiple-sensor estimations and described an approach to estimate the drift angle of multistory shear buildings from the measurements of one floor by using imprecisely identified parameters. In particular, a scheme of solving a constrained minimization problem is used to correct the mode shapes, striking a balance between the two aspects: (i) satisfying the orthogonality conditions as much as possible; (ii) ensuring that the calculated mode shapes will not deviate too much from the identified values (i.e., in an experience-based range). An experiment on a full-scale four-story shear structure was conducted in order to verify the proposed method. Modal parameters can be obtained by several methods from the recorded responses to small earthquakes or ambient vibrations with much less intensity. However, the identified parameters inevitably contain errors due to complex conditions, such as environmental effects, measurement noise, and so on. When many accelerometers are deployed, the large amount of data collected by them makes the response identification robust against modelling error and measurement noise. However, the performance dramatically drops off when observations on only one floor are available. By using the proposed algorithm, the accuracy of the mode shapes is enhanced and unrealistic vibrating shapes are avoided for the modal parameters containing errors, leading to a more accurate estimation of the drift angle.

When the accelerometer is deployed on the first floor, the responses of the lower floors can be obtained based on the more appropriate mode shapes. If more accurate results on the second or third floors are required, directly placing the sensors on the target floors turns out not to be the best idea because of the characteristic of the mode shapes of the shear structures for the single sensor-based estimation. The substructure approach can be used to transform the target story to “the ground story”, and the attempt will be made in the future. In addition, the identification of damping ratio usually has high uncertainty in the real environment, and especially the influence of damping ratio will increase when the frequency content of the signal is the same or similar to the structures. Therefore, the error in damping ratio will be dealt with to expand the application of the research.

Acknowledgments

The experimental data was from the E-Defense test, which was carried out at the National Research Institute for Earth Science and Disaster Resilience. The generosity of the staff at the institute in sharing their data is greatly appreciated. The study was partially supported by grants from the Japan Society for the Promotion of Science (JSPS KAKENHI 18H00968) and the Keio Leading-edge Laboratory 2021 Ph.D. Program Research Grant, and a scholarship, the ‘Design the Future’ Award of Keio University.

References

Al-Hussein, A. and Haldar, A. (2016), "Unscented Kalman filter with unknown input and weighted global iteration for health assessment of large structural systems", *Struct. Control Health Monitor.*, **23**(1), 156-175. https://doi.org/10.1002/stc.1764

Astroza, R., Ebrahimian, H., Conte, J.P., Restrepo, J.I. and Hutchinson, T.C. (2016), "System identification of a full-scale five-story reinforced concrete building tested on the NEES-UCSD shake table", *Struct. Control Health Monitor.*, **23**(3), 535-559. https://doi.org/10.1002/stc.1778

Azam, S.E., Chatzi, E. and Papadimitriou, C. (2015), "A dual Kalman filter approach for state estimation via output-only acceleration measurements", *Mech. Syst. Signal Process.*, **60**, 866-886. https://doi.org/10.1016/j.ymssp.2015.02.001

Brewick, P.T., Johnson, E.A., Sato, E. and Sasaki, T. (2018), "Constructing and evaluating generalized models for a base-isolated structure", *Struct. Control Health Monitor.*, **25**(11), e2243. https://doi.org/10.1002/stc.2243

Brincker, R., Zhang, L. and Andersen, P. (2001), "Modal identification of output-only systems using frequency domain decomposition", *Smart Mater. Struct.*, **10**(3), 441. https://doi.org/10.1088/0964-1726/10/3/303

Clough, R.W. and Penzien, J. (1993), *Dynamics of Structures*, (2nd edition), McGraw-Hill, New York, USA.

Dan, M., Ishizawa, Y., Tanaka, S., Nakahara, S., Wakayama, S. and Kohiyama, M. (2015), "Vibration characteristics change of a base-isolated building with semi-active dampers before, during, and after the 2011 Great East Japan earthquake", *Earthq. Struct., Int. J.*, **8**(4), 889-913. https://doi.org/10.12989/eas.2015.8.4.889

Das, S., Saha, P. and Patro, S.K. (2016), "Vibration-based damage detection techniques used for health monitoring of structures: a review", *J. Civil Struct. Health Monitor.*, **6**(3), 477-507. https://doi.org/10.1007/s13349-016-0168-5

Fan, W. and Qiao, P. (2011), "Vibration-based damage identification methods: a review and comparative study", *Struct. Health Monitor.*, **10**(1), 83-111. https://doi.org/10.1177/1475921710365419

Farrar, C.R., Baker, W.E., Bell, T.M., Cone, K.M., Darling, T.W., Duffey, T.A., Eklund, A. and Migliori, A. (1994), *Dynamic characterization and damage detection in the I-40 bridge over the Rio Grande*, No. LA-12767-MS, Los Alamos National Lab., NM, USA,

Gomez, F., Park, J.W. and Spencer Jr, B.F. (2018), "Reference-free structural dynamic displacement estimation method", *Struct. Control Health Monitor.*, **25**(8), e2209. https://doi.org/10.1002/stc.2209

Hyogo Earthquake Engineering Research Center [EB/OL]. https://www.bosai.go.jp/hyogo/research/project/steel0.html

Kang, J., Ju, H. and Liu, L. (2021), "Comparison of response transmissibility and power spectral density transmissibility on operational modal analysis", *Mech. Syst. Signal Process.*, **160**, 107912. https://doi.org/10.1016/j.ymssp.2021.107912

Khaloo, A. and Lattanzi, D. (2017), "Pixel-wise structural motion tracking from rectified repurposed videos", *Struct. Control Health Monitor.*, **24**(11), e2009. https://doi.org/10.1002/stc.2009

Kuleli, M. and Nagayama, T. (2020), "A robust structural parameter estimation method using seismic response measurements", *Struct. Control Health Monitor.*, **27**(3), e2475. https://doi.org/10.1002/stc.2475

Lei, Y., He, M., Liu, C. and Lin, S.Z. (2013), "Identification of tall shear buildings under unknown seismic excitation with limited output measurements", *Adv. Struct. Eng.*, **16**(11), 1839-1849. https://doi.org/10.1260/1369-4332.16.11.1839

Lei, Y., Xia, D., Erazo, K. and Nagarajaiah, S. (2019), "A novel unscented Kalman filter for recursive state-input-system identification of nonlinear systems", *Mech. Syst. Signal Process.*, **127**, 120-135. https://doi.org/10.1016/j.ymssp.2019.03.013

Li, Y., Luo, Y., Wan, H.P., Yun, C.B. and Shen, Y. (2020), "Identification of earthquake ground motion based on limited acceleration measurements of structure using Kalman filtering technique", *Struct. Control Health Monitor.*, **27**(1), e2464. https://doi.org/10.1002/stc.2464

Liang, W., Huang, J. and Zhang, J. (2020), "Comparison of Displacement Reconstruction Methods by Acceleration Measurement", *Proceedings of the Seventh Asia International Symposium on Mechatronics*, Singapore.

Liu, X., Wang, Y. and Verriest, E.I. (2021), "Simultaneous input-state estimation with direct feedthrough based on a unifying MMSE framework with experimental validation", *Mech. Syst. Signal Process.*, **147**, 107083. https://doi.org/10.1016/j.ymssp.2020.107083

Lourens, E., Reynders, E., De Roeck, G., Degrande, G. and Lombaert, G. (2012), "An augmented Kalman filter for force identification in structural dynamics", *Mech. Syst. Signal Process.*, **27**, 446-460. https://doi.org/10.1016/j.ymssp.2011.09.025

Maes, K., Smyth, A.W., De Roeck, G. and Lombaert, G. (2016), "Joint input-state estimation in structural dynamics", *Mech. Syst. Signal Process.*, **70**(445-466). https://doi.org/10.1016/j.ymssp.2015.07.025

Maksymenko, O.P., Sakharuk, O.M., Ivanytskyi, Y.L. and Kun, P.S. (2021), "Multilaser spot tracking technology for bridge structure displacement measuring", *Struct. Control Health Monitor.*, **28**(3), e2675. https://doi.org/10.1002/stc.2675

Mao, J.X., Wang, H., Fu, Y.G. and Spencer Jr, B.F. (2019), "Automated modal identification using principal component and cluster analysis: Application to a long-span cable-stayed bridge", *Struct. Control Health Monitor.*, **26**(10), e2430. https://doi.org/10.1002/stc.2430

Mendrok, K. and Dworakowski, Z. (2019), "A review of methods for excitation force reconstruction", *Diagnostyka*, **20**(11-19). https://doi.org/10.29354/diag/110241

Mita, A. (2003), *Structural Dynamics for Health Monitoring*, Sankeisha, Nagoya, Japan.

Nayek, R., Chakraborty, S. and Narasimhan, S. (2019), "A Gaussian process latent force model for joint input-state estimation in linear structural systems", *Mech. Syst. Signal Process.*, **128**, 497-530. https://doi.org/10.1016/j.ymssp.2019.03.048

Pan, S., Xiao, D., Xing, S., Law, S.S., Du, P. and Li, Y. (2016), "A general extended Kalman filter for simultaneous estimation of system and unknown inputs", *Eng. Struct.*, **109**, 85-98. https://doi.org/10.1016/j.engstruct.2015.11.014

Sedehi, O., Papadimitriou, C., Teymouri, D. and Katafygiotis, L.S. (2019), "Sequential Bayesian estimation of state and input in dynamical systems using output-only measurements", *Mech. Syst. Signal Process.*, **131**, 659-688. https://doi.org/10.1016/j.ymssp.2019.06.007

Sen, S. and Bhattacharya, B. (2017), "Online structural damage identification technique using constrained dual extended Kalman filter", *Struct. Control Health Monitor.*, **24**(9), e1961. https://doi.org/10.1002/stc.1961

Shrestha, A., Dang, J., Nakajima, K. and Wang, X. (2020), "Image processing–based real-time displacement monitoring methods using smart devices", *Struct. Control Health Monitor.*, **27**(2), e2473. https://doi.org/10.1002/stc.2473

Sun, L., Li, Y., Zhu, W. and Zhang, W. (2020), "Structural response reconstruction in physical coordinate from deficient measurements", *Eng. Struct.*, **212**(110484). https://doi.org/10.1016/j.engstruct.2020.110484

Taher, S.A., Li, J. and Fang, H. (2020), "Online input, state, and response estimation for building structures under earthquakes using limited acceleration measurements", *Proceedings Sensors and Smart Structures Technologies for Civil*, *Mechanical*, *and Aerospace Systems 2020*, Vol. 11379, pp. 42-50.

Valikhani, M. and Younesian, D. (2019), "Bayesian framework for simultaneous input/state estimation in structural and mechanical systems", *Struct*. *Control Health Monitor*., **26**(9), e2379. https://doi.org/10.1002/stc.2379

Van Overschee, P. and De Moor, B.L. (2012), Subspace identification for linear systems: Theory—Implementation—Applications, Springer Science & Business Media.

Wu, M. and Smyth, A.W. (2007), "Application of the unscented Kalman filter for real-time nonlinear structural system identification", *Structural Control and Health Monitoring*: *The Official Journal of the International Association for Structural Control and Monitoring and of the European Association for the Control of Structures*, **14**(7), 971-990. https://doi.org/10.1002/stc.186

Xie, B., Li, J. and Zhao, X. (2021), "Accuracy and sensibility analysis of strain measurement based on microimages captured by smartphone with a microscope", *Struct*. *Control Health Monitor*., **28**(3), e2692. https://doi.org/10.1002/stc.2692

Xu, K. and Mita, A. (2021a), "Estimation of maximum drift of multi-degree-of-freedom shear structures with unknown parameters using only one accelerometer", *Struct*. *Control Health Monitor*., **28**(9), e2799. https://doi.org/10.1002/stc.2799

Xu, K. and Mita, A. (2021b), "Maximum drift estimation based on only one accelerometer for damaged shear structures with unknown parameters", *J. Build*. *Eng*., 103372. https://doi.org/10.1016/j.jobe.2021.103372

Xu, K. and Mita, A. (2021c), "Absolute displacement-based formulation for peak inter-story drift identification of shear structures using only one accelerometer", *Sensors*, **21**(11), 3629. https://doi.org/10.3390/s21113629

Xu, Y., Brownjohn, J. and Kong, D. (2018), "A non-contact vision-based system for multipoint displacement monitoring in a cable-stayed footbridge", *Struct*. *Control Health Monitor*., **25**(5), e2155. https://doi.org/10.1002/stc.2155

Yang, Y., Nagayama, T. and Xue, K. (2020), "Structure system estimation under seismic excitation with an adaptive extended kalman filter", *J. Sound Vib*., **489**, 115690. https://doi.org/10.1016/j.jsv.2020.115690

Zhang, L., Liu, P., Yan, X. and Zhao, X. (2020), "Middle displacement monitoring of medium–small span bridges based on laser technology", *Struct*. *Control Health Monitor*., **27**(4), e2509. https://doi.org/10.1002/stc.2509

Zhao, X., Xu, Y.L., Chen, J. and Li, J. (2005), "Hybrid identification method for multi-story buildings with unknown ground motion: Experimental investigation", *Eng*. *Struct*., **27**(8), 1234-1247. https://doi.org/10.1016/j.engstruct.2005.03.008

Appendix A

The state-space equation in continuous time is

$$\dot{\boldsymbol{x}}_k = \boldsymbol{A}_c \boldsymbol{x}_k + \boldsymbol{B}_c p_k + \boldsymbol{w}_k^x \tag{A1}$$

$$y_k = \boldsymbol{H}_c \boldsymbol{x}_k + v_k \tag{A2}$$

$$\boldsymbol{z}_k = \boldsymbol{L}_c \boldsymbol{x}_k \tag{A3}$$

where

$$\boldsymbol{x}_k = [v_1(k) \quad \dot{v}_1(k) \quad \cdots \quad \cdots \quad v_n(k) \quad \dot{v}_n(k)]^T$$

$$\boldsymbol{A}_c = \begin{bmatrix} 0 & 1 & & & & 0 \\ -\omega_1^2 & -2\xi_1\omega_1 & & & & \\ & & \cdots & \cdots & & \\ & & \cdots & \cdots & & \\ & & & & 0 & 1 \\ 0 & & & & -\omega_n^2 & -2\xi_n\omega_n \end{bmatrix}$$

$$\boldsymbol{B}_c = [0 \quad -1 \quad \cdots \quad \cdots \quad 0 \quad -1]^T$$

$$\boldsymbol{H}_c = [\omega_1^2\phi_{i1}\Gamma_1 \quad 0 \quad \cdots \quad \cdots \quad \omega_n^2\phi_{in}\Gamma_n \quad 0]^T$$

$$\boldsymbol{L}_c = \begin{bmatrix} \phi_{11}\Gamma_1 & 0 & \cdots & \cdots & \phi_{1n}\Gamma_n & 0 \\ \phi_{21}\Gamma_1 & 0 & \cdots & \cdots & \phi_{2n}\Gamma_n & 0 \\ \vdots & \vdots & \ddots & \ddots & \vdots & \vdots \\ \phi_{n1}\Gamma_1 & 0 & \cdots & \cdots & \phi_{nn}\Gamma_n & 0 \end{bmatrix}$$

$$\Gamma_j = \phi_j^T \boldsymbol{M}\boldsymbol{r}$$

$v_j(t)$ and $\dot{v}_j(t)$ are modal displacement response and modal velocity response, ω_j, ξ_j and ϕ_j represent natural frequency, damping ratio, and mode shapes, $\boldsymbol{M}$ is the mass matrix, $\boldsymbol{r}$ denotes an $n \times 1$ unit vector ($r = [1 \quad \cdots \quad 1]^T$), $\boldsymbol{w}_k^x$ and v_k are the process noise and measurement noise with known covariance matrices $\boldsymbol{Q}^x$ and $\boldsymbol{R}$.

The state-space matrices in discrete time can be obtained

$$\begin{aligned} &\boldsymbol{A} = exp(\boldsymbol{A}_c \Delta t), \quad \boldsymbol{B} = (\boldsymbol{A} - \boldsymbol{I})\boldsymbol{A}_c^{-1}\boldsymbol{B}_c, \\ &\boldsymbol{H} = \boldsymbol{H}_c, \quad \boldsymbol{L} = \boldsymbol{L}_c \end{aligned} \tag{A4}$$

The Kalman filter is shown in Table A1.

Table A1 Two-stage filter for the input and state estimation

1. Initialization

$\boldsymbol{x}_{0|0}$, $\boldsymbol{P}_{0|0}^x$, p_{-1}, $\boldsymbol{P}_{-1|-1}^p$, $\boldsymbol{Q}^x$, $\boldsymbol{Q}^p$, $\boldsymbol{R}$

2. Time update of input

$$p_{k|k-1} = p_{k-1|k-1}$$
$$\boldsymbol{P}_{k|k-1}^p = \boldsymbol{P}_{k-1|k-1}^x + \boldsymbol{Q}^p$$

3. Measurement update of input

$$\boldsymbol{G}_k^p = \boldsymbol{P}_{k|k-1}^p(\boldsymbol{H}\boldsymbol{B})^T[(\boldsymbol{H}\boldsymbol{B})\boldsymbol{P}_{k|k-1}^x(\boldsymbol{H}\boldsymbol{B})^T + \boldsymbol{R}]^{-1}$$
$$p_{k|k} = p_{k|k-1} + \boldsymbol{G}_k^p(\boldsymbol{y}_{k+1} - \boldsymbol{H}\boldsymbol{A}\boldsymbol{x}_{k|k} - \boldsymbol{H}\boldsymbol{B}p_{k|k-1})$$
$$\boldsymbol{P}_{k|k}^p = (\boldsymbol{I} - \boldsymbol{G}_k^p\boldsymbol{B})\boldsymbol{P}_{k|k-1}^p$$

4. Time update of state

$$\boldsymbol{x}_{k+1|k} = \boldsymbol{A}\boldsymbol{x}_{k|k} + \boldsymbol{B}p_{k|k}$$
$$\boldsymbol{P}_{k+1|k}^x = \boldsymbol{A}\boldsymbol{P}_{k|k}^x\boldsymbol{A}^T + \boldsymbol{Q}^x$$

5. Measurement update of state

$$\boldsymbol{G}_{k+1}^x = \boldsymbol{P}_{k+1|k}^x\boldsymbol{H}^T(\boldsymbol{H}\boldsymbol{P}_{k+1|k}^x\boldsymbol{H}^T + \boldsymbol{R})^{-1}$$
$$\boldsymbol{x}_{k+1|k+1} = \boldsymbol{x}_{k+1|k} + \boldsymbol{G}_{k+1}^x(\boldsymbol{y}_{k+1} - \boldsymbol{H}\boldsymbol{x}_{k+1|k})$$
$$\boldsymbol{P}_{k+1|k+1}^x = (\boldsymbol{I} - \boldsymbol{G}_{k+1}^x\boldsymbol{H})\boldsymbol{P}_{k+1|k}^x$$